

RSC Advances



This is an *Accepted Manuscript*, which has been through the Royal Society of Chemistry peer review process and has been accepted for publication.

Accepted Manuscripts are published online shortly after acceptance, before technical editing, formatting and proof reading. Using this free service, authors can make their results available to the community, in citable form, before we publish the edited article. This *Accepted Manuscript* will be replaced by the edited, formatted and paginated article as soon as this is available.

You can find more information about *Accepted Manuscripts* in the [Information for Authors](#).

Please note that technical editing may introduce minor changes to the text and/or graphics, which may alter content. The journal's standard [Terms & Conditions](#) and the [Ethical guidelines](#) still apply. In no event shall the Royal Society of Chemistry be held responsible for any errors or omissions in this *Accepted Manuscript* or any consequences arising from the use of any information it contains.



Enhancement of physicochemical properties of polyurethane-perovskite nanocomposite *via* addition of nickel titanate nanoparticles

Received 00th January 20xx,
Accepted 00th January 20xx

DOI: 10.1039/x0xx00000x

www.rsc.org/

Adhigan Murali,^a Senthil A. Gurusamy-Thangavelu,^{a,*} Sellamuthu N. Jaisankar,^{a,*} and Asit Baran Mandal^{a,b*}

Polyurethane (PU)-perovskite nanocomposite films were developed by *in situ* addition of nickel titanate nanoparticles (NiTiO₃ NPs) into PU matrix formulation. Among the three samples of NiTiO₃ NPs calcinated at 400, 600 and 800 °C, the pertinent rhombohedral phase of NiTiO₃ has been achieved at 800 °C. NiTiO₃ is loaded in trace amount (0.5 wt. %) with PU matrix to cast as films (thickness, ~1.5 mm), which demonstrate its influence on PU, studied by ATR-IR, Raman, UV-*vis* DRS, XRD, TGA, DSC, XPS, AFM, SEM, optical microscopy, vibrating sample magnetometer (VSM) and impedance spectroscopy. The characteristics of PU-NiTiO₃ nanocomposite films are compared with control PU film, these reveal the enhancement in thermal stability (>10 °C), electrical conductivity (8.72 x 10⁻⁵ S cm⁻¹) and mechanical strength (19.7±0.8 MPa) as well as the effect in magnetic and optical properties due to non-covalent interaction upon uniform distribution of NiTiO₃ on PU film.

1. Introduction

Inorganic functional materials such as metal oxides and perovskites with ABO₃ type structure, MTiO₃ (M = Ni, Pb, Fe, Co, Cu and Zn) were used widely in diverse applications.¹⁻⁵ Due to their optical,⁶ piezoelectric,⁷ magnetic,⁸ photocatalyst,^{9,10} and catalytic¹¹ properties, often explored in solar cell,^{12,13} energy storage,¹⁴ fuel cell,¹⁵ waste water treatment,¹⁶ gas sensor,¹⁷ coating to reduce friction and lubrication,^{18,19} corrosion inhibitor²⁰ and pigment.²¹ Typically, integration of inorganic materials with polymer can afford variety of nanocomposite, accomplished by melt compounding, film casting and *in situ* polymerization.²²

Currently, nickel titanate nanoparticles (NiTiO₃ NPs) is incorporated with polyurethane (PU) matrix by *in situ* addition to develop an unprecedented nanocomposite, PU-NiTiO₃. It shows the enhanced physicochemical properties as similar to other known nanocomposites.²³⁻²⁸ Our previous reports focus on siloxane crosslinked PU composite,²⁹ degradation of dye using perovskite³⁰ and polymerization on self-assembled

monolayer³¹ as well as nanocomposite based on silica NPs³² and single-walled carbon nanotubes (SWCNTs).^{33,34} In our recent report, (OH)_n-SWCNTs (0.01 - 0.3 wt. %) was loaded *via* covalent addition to afford PU-(OH)_n-SWCNTs with enhancement of thermal, conductivity, mechanical and magnetic properties.³⁵ At present, PU-NiTiO₃ from PU and NiTiO₃ is generated originally to exemplify the influence of NiTiO₃ on PU. The pure inorganic nanomaterial, NiTiO₃ has been loaded with PU matrix to enhance the physicochemical properties. This composite is considered to be significant due to its simple approach to incorporate the viably synthesized NiTiO₃ NPs (0.5 wt. %) *via* non-covalent interaction. The new strategy for the uniform distribution of cost effective NiTiO₃ on PU is aiming to replace the influence of the expensive nanomaterial, (OH)_n-SWCNTs (functionalization of SWCNTs by mild synthetic route) on PU *via* covalent bond.³⁵

Synthesis of NiTiO₃ by the conventional solid state method is hampered due to high sintering temperatures and poor composition homogeneity. However, sol-gel/co-precipitation method carry advantages such as stoichiometric control, purity and easy to coat/distribute on films.^{36,37} NiTiO₃ is known for its propensity to reduce friction and wear in tribological coating, found to minimize the friction and wear over the wide range of temperature instead of conventional liquid/solid lubricants.¹⁸ Also, it is considered taking advantage of electrical properties of 3d transition perovskite and semiconducting metal oxide, NiTiO₃, towards the objective to improve the conductivity of PU.³⁸ In principle, the electrical properties of such materials depends upon the narrow 3d bands of respective transition metal ions.

^aPolymer Division and ^bChemical laboratory, Council of Scientific and Industrial Research (CSIR)-Central Leather Research Institute (CLRI), Adyar, Chennai-600 020, Tamil Nadu, India

*E-mail: senthil@clri.res.in; snjsankar@clri.res.in; abmandal@clri.res.in; Tel: 91-44-24422059; Fax:91-44-24911589.

†Electronic Supplementary Information (ESI) available: Raman spectra, SEM, optical microscopic images and three dimensional AFM images of PU, NiTiO₃ NPs and PU-NiTiO₃ as well as the tensile profile of PU and PU-NiTiO₃ films. See DOI: 10.1039/x0xx00000x

Despite the polymer-perovskite type composites like PU-TiO₂,³⁹ poly(vinyl acetate)-NiTiO₃⁴⁰ and poly(imide)-NiTiO₃⁴¹ are synthesized by *in situ* polymerization and electrospinning method,⁴² such composites tend to manifest the enhancement of selective physical properties only. Indeed, NiTiO₃ is explored to reinforce the physicochemical properties of PU for the first time to our knowledge. Similar examples, chloropolyaniline-NiTiO₃ has been formed by *in situ* polymerization, wherein NiTiO₃ reduced the electrical resistance of the polymer.⁴³ In case of PU-KTiO₃, it exhibits the improvement in mechanical properties.⁴⁴

It is ubiquitous that nanocomposites employ towards the specific purpose in electronic, optical, thermal, mechanical and magnetic properties. In spite of the typical variation of nanomaterial loading range (0.5 to 10 %) in polymer nanocomposite,⁴⁵ least range of NiTiO₃ (0.5 wt. %) is chosen to load in PU pre-polymer to study the augmentation of thermal, electrical and mechanical properties, beside its suppression in magnetism.⁴⁶ As compared to previous reports on polymer-NiTiO₃, unique features of PU-NiTiO₃ is that the addition of NiTiO₃ with PU leads to the enhancement of multiple physicochemical properties concurrently rather than specifically. Altogether, the viably synthesized cost effective NiTiO₃ employs as potential nanomaterial in the present study.

2. Experimental

2.1. Materials

Poly(propylene glycol) (PPG, average M_n ~ 2000), toluene-2,4-diisocyanate (TDI, 80 %) and dibutyltin dilaurate (DBTDL) were procured from Aldrich, USA. Nickel (II) chloride hexahydrate (NiCl₂·6H₂O), Titanium tetrachloride (TiCl₄), N-Cetyl- N, N, N-trimethyl-ammonium bromide (CTAB), Tetrahydrofuran (THF), 2-methoxy ethanol and sodium hydroxide (NaOH) pellets were purchased from Merck. Freshly distilled dry THF (after stored overnight in sodium hydroxide) was added in PU formulation. Poly(propylene glycol) was dried in rotavapor at 70 °C for 1 h and purged with nitrogen before charged in RB flask for the formulation.

2.2. Characterization methods

The ATR-IR accessory was mounted in ABB MB3000 laboratory FT-IR spectrometer to collect spectra for the PU and PU-NiTiO₃ nanocomposite films, while nickel titanate samples were analyzed by KBr pellet method. Confocal Raman spectrometer (Nanophoton Corporation, Japan), equipped with N₂ laser (excited at 532 nm) was used to record Raman spectral data. FEI Quanta 200 FEG has been operated at 15 kV in high vacuum to analyse morphology by SEM. AFM imaging on these films surface was conducted by NT-MDT (NTEGRA Prima, Netherlands). XPS analysis on NiTiO₃ NPs was performed with small spot capability (<15 microns) by AXIS ULTRA using microchannel plate and phosphor detection system. UV-vis DRS spectra of these four film samples were characterized by LAMBDA 650 UV-vis spectrometer. Magnetic characteristics of NiTiO₃ and nanocomposite films were deduced from the data

acquired from the Lake Shore 7410 vibrating sample magnetometer (VSM). OLYMPUS BX50 with transmitted light (DIC /NOMARSKI & UPLANFL 4X, 10X, 20X, 40X & 100X objectives) was used to record the optical microscopic images. DSC thermal study was conducted between the temperature range, 25 to 300 °C by DSC Q200, TA-Instruments. TGA thermogram for the same samples was recorded from Q50 TGA, TA Instruments. Crystalline phase formation of NiTiO₃ as well as PU and PU-NiTiO₃ films were analysed by X-ray diffraction analysis by X-ray diffractometer, Rigaku Miniflex using CuK_{α1} radiation. The conductivity data was recorded by impedance spectroscopy, Hewlett Packard 4284A Precision LCR Meter. Tensile strength measurements have been carried out by Instron Testing Machine, Model #3369, Instron Corporation, Norwood, MA, USA. Probe sonicator, Sonics VCX 750 (750 W, 20 KHz), Sonics & materials Inc., Newtown, USA was operated at 60 % amplitude to prepare the dispersion of NiTiO₃ NPs in THF.

2.3. Synthetic formulation of PU pre-polymer (control)

PU was formulated as pre-polymer in a three-necked RB flask, equipped with a mechanical stirrer, under nitrogen atmosphere. RB flask was charged with poly(propylene glycol) (4.5 g, 0.00225 M) and toluene-2,4-diisocyanate (TDI, 2.5 mL, 0.0139 M) at ambient temperature. To the above stirred reaction mixture, DBTDL (0.025 g, 0.000144 M) and dry THF (3 mL) were added before ramping the oil bath temperature up to 65 °C. This reaction mixture was maintained at 65 °C under stirring for 2 h and periodic additions of dry THF (3 mL) was continued for every 15 min., prevented any gel formation. This viscous and translucent reaction mixture was removed from the oil bath and immediately distributed homogeneously on glass petri dish to cast as uniform film (thickness ~1.5 mm). The film was subjected to moisture curing at ambient temperature for a week.^{35,47,48}

2.4. Synthetic formulation of PU-nickel titanate nanocomposite

To synthesize the PU nanocomposite, PU pre-polymer was reproduced by the above experimental procedure (see section 2.3). *In situ* addition of NiTiO₃ NPs (calcinated at 800 °C) was continued in the same three-necked reaction flask to convert into PU-NiTiO₃ nanocomposite. The dispersion of NiTiO₃ NPs (0.035 g, 0.5 wt. %) in dry THF (5 mL) was treated for ultrasonication about 30 min. and transferred into the viscous medium of PU pre-polymer stirred at 1000 rpm in oil bath maintained at 65 °C. PU-NiTiO₃ nanocomposite reaction mixture has been stirred for 30 min. and removed from the oil bath. This product was immediately distributed uniformly on petri dish to cast as film. Nanocomposite film, PU-NiTi800 was allowed undergo moisture curing at ambient temperature for a week, before subjected to further analysis. Similar procedure was repeated to develop PU-NiTiO₃ nanocomposite films using NiTiO₃ NPs (calcinated at 400 and 600 °C, 0.5 wt. %) to cast the other two nanocomposite films, PU-NiTi400 and PU-NiTi600.

2.5. Synthesis of nickel titanate nanoparticles (NiTiO₃ NPs)

Nickel chloride (9.6 g) was dissolved in deionized water (20 mL) using a beaker (100 mL) over the period of 20 min. at ambient

temperature. CTAB (2.2 g) was dissolved thoroughly using deionized water (20 mL) and hydrochloric acid (1 mL) in another beaker (100 mL). CTAB solution was added drop wise for 5 min. to the solution of nickel chloride. To the above mixture, sodium hydroxide (10 g) dissolved in deionized water (20 mL) was added drop wise under stirring for 30 min. to obtain homogeneous solution. Once again, CTAB (2.2 g) solution was prepared using deionized water (20 mL) and drop wise addition of hydrochloric acid (1 mL) has been done for the period of 5 min. This was added into the solution of titanium chloride (15 g) dispersed in 2-methoxy ethanol (20 mL) and continued to stir for 20 min. $\text{Ti}(\text{OCH}_2\text{CH}_2\text{OCH}_3)_4$ generated⁴⁹ from the above mixture has been transferred using a dropping funnel for 15 min. into $\text{Ni}(\text{OH})_2$ solution. Ammonium hydroxide (25 % aqueous ammonia solution, 17 mL) was added slowly to the above reaction mixture, stirred for 2 h to obtain the precipitate.

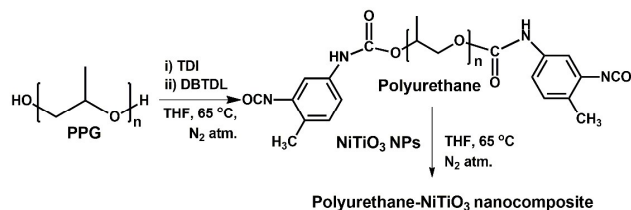
The above precipitate was filtered using Whatman filter paper and washed using deionized water about 10 times, the precipitate dried in oven at 100 °C for 5 h to obtain as powder. As synthesized nickel titanate was subjected to calcination process in a closed quartz crucible at 400, 600 and 800 °C under air atmosphere for 4 h.

3. Results and Discussion

Herein, NiTiO_3 NPs by sol-gel/co-precipitation method was integrated by *in situ* addition with PU pre-polymer to form the PU- NiTiO_3 nanocomposite. Amidst the variety of synthetic methods (hydrothermal,⁵⁰ chemical,^{21,51} microwave-assisted,⁵² sol-gel/co-precipitation,^{53,37} nanoparticle directed,⁵⁴ sonochemical,⁵⁵ solvothermal⁵⁶ electrochemical,⁵⁷ polymer precursor,⁵⁸ Pechini's process⁵⁹ and molten salt⁸) available for the preparation of NiTiO_3 NPs, sol-gel/co-precipitation method was adopted to obtain from the nickel (II) and titanium (IV) precursors *via* co-precipitation. Further upon calcination in atmospheric air at 400, 600 and 800 °C for 4h, which is illustrated in flow chart given in scheme S1 (ESI). To characterize preliminarily, optical microscopic images were collected as given in Fig. S3 (ESI), exhibit the formation of spherical nanoparticles with wide distribution of particle sizes. SEM images in Fig. S4 (ESI) depicts the size distribution of NiTiO_3 NPs, range between 100 nm-1 μm . Despite the calcination has been initiated to generate the pure NiTiO_3 from 400 °C, the appropriate product started to form at 600 °C, according to Raman data shown in Fig. S1. Essentially, the peaks position in Raman spectrum of NiTiO_3 vary depends on the synthetic procedure, average crystal size and degree of structural order in crystal.³⁶ Further elevation of calcination temperature up to 800 °C has afforded the pertinent phase of NiTiO_3 sample, free from NiO and TiO_2 .³⁹ TGA profile of the NiTiO_3 was recorded to identify the onset degradation temperature at 228 °C, as presented in Fig. S2.³⁶

However, the evidence for the accurate formation of NiTiO_3 as rhombohedral phase at 800 °C was supported by XRD peaks. PPG polyol ($f_n=2$, average $M_n \sim 2000$) has been chosen to formulate the PU matrix using the highly reactive isocyanate reagent, TDI for

casting PU film (thickness ~ 1.5 mm). PU- NiTiO_3 film was obtained by *in situ* addition of NiTiO_3 NPs (0.5 wt. %) into the viscous medium of PU pre-polymer to obtain nanocomposite, as shown in scheme 1.



Scheme 1 Synthesis of PU and PU- NiTiO_3 nanocomposite film samples, PU-NiTi400, PU-NiTi600 and PU-NiTi800.

The physicochemical and morphological properties of NiTiO_3 NPs as well as PU and PU- NiTiO_3 nanocomposite films were characterized by ATR-IR, Raman, UV-*vis* DRS, XRD, TGA, DSC, XPS, AFM, SEM, optical microscopy, impedance spectroscopy, vibrating sample magnetometer (VSM) and tensile measurements. ATR-IR and Raman data in Fig. 1, deduce the functionality and molecular structure of these films. ATR-IR spectra of PU determines the axial stretching frequencies of urethane link at 3310 cm^{-1} (NH) and 1720 cm^{-1} (C=O). Symmetric stretching vibration of methyl (CH₃) is noticed at 2980 cm^{-1} and strong absorption at 1095 cm^{-1} is assigned for the C-O-C moiety of PPG polyol. Aromatic (C=C) bending (1657 cm^{-1}) and aromatic (C-H) bending (769 cm^{-1}) vibrations infer the presence of TDI, as shown in Fig. 1a.²⁵

Moreover, ATR-IR spectra was collected for the other three nanocomposite films and compared with control PU film. All characteristic vibrational frequencies correspond to PU- NiTiO_3 films slightly shift relative to PU film [Table S1] due to non-covalent interaction. Raman spectral data is depicted in Fig. 1b, which identify the formation of urethane bonds as well as the dispersion of NiTiO_3 on PU- NiTiO_3 films.

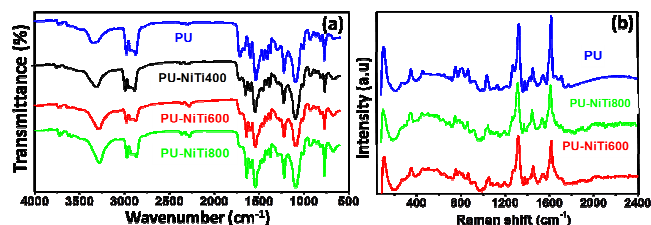


Fig. 1 a) ATR-IR spectra of PU control and PU- NiTiO_3 nanocomposite films, b) Raman spectra of PU control and nanocomposite films.

In particular, amide III (1260 cm^{-1}) and C=O (1710 cm^{-1}) group signals are disrupted in PU- NiTi600 and PU- NiTi800 and no shift in spectral band is noticed with amide II (1541 cm^{-1}) peak of these nanocomposite films. The signals of amide I band of PU- NiTi800 (1648 cm^{-1}) and PU- NiTi600 (1630 cm^{-1}) is shifted relative to PU (1615 cm^{-1}).²⁵ More peaks are detected in Fig. 1b, with respect to asymmetric deformation of CH₃ group at 1454 cm^{-1} , aromatic ring deformation at 1040 cm^{-1} and C-O-C moiety at 868 cm^{-1} .^{35, 60}

ARTICLE

In addition to the characterization of these films by ATR-IR and Raman spectra, NiTiO₃ NPs samples treated at 400, 600 and 800 °C were characterized by FT-IR to show the appropriate formation of the sample. In FT-IR data of NiTiO₃, the spectral region between 1000-500 cm⁻¹ is magnified and included in Fig. 2a. This exhibit a broad band around 600-625 cm⁻¹ to identify the stretching mode of Ti-O and O-Ti-O bending mode as characteristic of NiTiO₃ calcinated at 600 and 800 °C.⁴⁰ It is essential to collect UV-vis DRS data on film samples to study their physicochemical properties. To indicate the interface of NiTiO₃ NPs on PU-NiTiO₃ films, absorption values are analysed from Fig. 2b. The specific absorption peaks of these films are noticed in the visible region (400-800 nm), PU-NiTi400 (λ_{max}=519 nm), PU-NiTi600 (λ_{max}=549 nm) and PU-NiTi800 (λ_{max}=551 nm), justify the interfacial interaction of NiTiO₃ with PU.

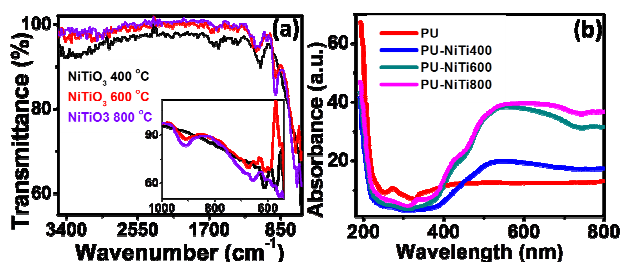


Fig. 2 a) FT-IR of NiTiO₃ samples calcinated at 400, 600 and 800 °C with inset for the region (1000-500 cm⁻¹) and b) UV-vis DRS data of PU, PU-NiTi400, PU-NiTi600 and PU-NiTi800.

The prominent shift in the absorption amidst PU-NiTi400 (519 nm) and PU-NiTi600 (549 nm) seems to be indicative of the formation of NiTiO₃ at 600 °C rather than at 400 °C. NiTiO₃ NPs is loaded in PU-NiTi800 (551 nm), after calcinated at 800 °C (Ni²⁺ and Ti⁴⁺ solely transformed to NiTiO₃). The occurrence of inter-valence charge transfer from Ni²⁺ to Ti⁴⁺ is noticed as absorption in the visible region (519, 549 and 551 nm) as per the graph depicted in Fig. 2b.^{8,40,59} No such absorption was observed in the control PU.

Apart from the FT-IR data of NiTiO₃ (Fig. 2a), characterization by X-ray diffraction (XRD) peak pattern is essential to elucidate the specific feature of these samples. To evaluate the crystal phases, XRD patterns were recorded on powder sample and shown in Fig. 3a. XRD peaks of powder calcinated at 800 °C suggest a significant formation of NiTiO₃. In Fig. S1, Raman data supports the initiation to form NiTiO₃ at 600 °C. Further raise in calcination temperature up to 800 °C favours the formation of NiTiO₃, free from NiO and TiO₂. The above data corroborates the authentic formation of rhombohedral phase, according to the standard data set verified from JCPDS file number 33-690.⁴⁰ XRD peak patterns of NiTiO₃, PU and PU-NiTi800 samples are compared in Fig. 3a, where the peak patterns of PU-NiTi800 appear as the overlapped peaks of PU and NiTiO₃, supported the encapsulation of NiTiO₃ NPs into PU matrix.

The intrinsic modification in electrical properties of the nanocomposite is investigated by the impedance spectroscopy. Since the NiTiO₃ is comprised of narrow 3d bands, electrical conductivity is entailed of complex mechanism. The conductivity of NiTiO₃ NPs is determined by the electronic energy bands associated

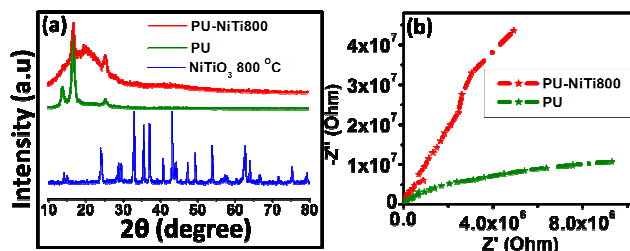


Fig. 3 a) XRD patterns of NiTiO₃ calcinated at 800 °C, PU and PU-NiTi800 and b) Impedance spectroscopy data of PU and PU-NiTi800.

with conduction of Ni²⁺ (3d⁸), Ti⁴⁺ (3d⁰) and O²⁻ (2p⁶).³⁸ Impedance data was collected on PU and PU-NiTi800 in order to compare their conductivity in Fig. 3b. The real (Z') and imaginary (Z'') impedance values were noted from these measurements at room temperature and plotted in Fig. 3b. Despite the trace of NiTiO₃ (0.5 wt. %) is incorporated in PU-NiTi800, enhanced the specific conductivity (8.72 × 10⁻⁵ S cm⁻¹), two order higher than the conductivity (9.38 × 10⁻⁷ S cm⁻¹) of PU, as shown in Fig. 3b.³⁵ The enhancement in conductivity value matches with our previous report, wherein nanocomposite formed between PU and (OH)_n-SWCNTs.³⁵

Thermogravimetric analysis (TGA) was conducted to study the improvement in thermal properties. TGA of PU and PU-NiTiO₃ film exemplifies the effect of NiTiO₃ NPs on PU film to enhance its thermal stability as shown in Fig. 4a. As such PU exhibits the onset degradation temperature at 415 °C while the other PU-NiTiO₃ fairly shift its degradation temperature, PU-NiTi400 (421 °C), PU-NiTi600 (423 °C) and PU-NiTi800 (426 °C), respectively.⁴⁵ The char residue for the PU remains 2.1 %, which exists less than the residue value of other three nanocomposite films, 3.5-5 %. The above degree of improvement in thermal stability (>10 °C) of PU-NiTiO₃ is also coincide with the results of PU-(OH)_n-SWCNTs.³⁵

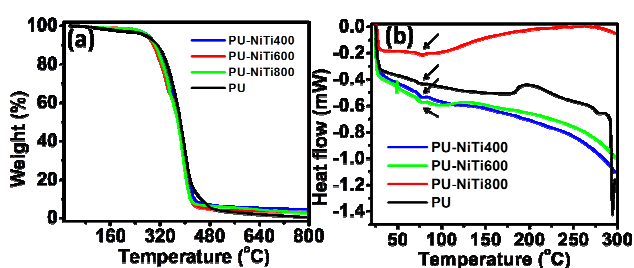


Fig. 4 a) TGA data of PU, PU-NiTi400, PU-NiTi600 and PU-NiTi800 and b) DSC profile for PU and PU-NiTiO₃ nanocomposite (arrows indicate the region of glass transition temperature).

Differential scanning calorimetric (DSC) analysis results of these samples are shown in Fig. 4b. In all four DSC profiles, including PU and three nanocomposite samples, single T_g value was noticed around 77 °C. In particular, PU only reveals the melting behavior beyond 290 °C, whereas such decomposition was not identified in nanocomposite samples. DSC data is shown in Fig. S19 (ESI), wherein the certain glass transition behaviour is noticed in the expanded region of each profile. Since the NiTiO₃ interact efficiently with PU, nanocomposite films reveal the enhancement of thermal

stability upon incorporation of NiTiO₃. DSC results of PU-NiTiO₃ did not show any shift in T_g value as relative to PU, similar trend was observed with PU-(OH)_n-SWCNTs nanocomposite as well.³⁵

Followed by encouraging results observed with electrical conductivity and thermal stability, prompted us to examine the mechanical properties of these films.⁶¹ Tensile parameters were measured on these films by the universal testing machine, which suggest the influence of NiTiO₃ NPs to enhance the tensile strength of PU films,⁴¹ these are measured similar to PU incorporated with SWCNTs.³⁵ The tensile strength of these samples increase gradually from entry 1 (17.1±0.9 MPa) to entry 4 (19.7±0.8 MPa) as listed in Table 1. Tensile profile of these samples is depicted in Fig. S15-S18.

Table 1. Mechanical properties of PU and PU-NiTiO₃ films.

S. No.	Sample codes	Tensile strength [MPa]	Young's modulus [MPa]	Elongation at break (%)
1	PU	17.1±0.9	2.78±0.4	392.3±36
2	PU-NiTi400	17.6±1.2	1.66±0.6	680.3±42
3	PU-NiTi600	18.0±1.1	1.63±0.6	735.3±40
4	PU-NiTi800	19.7±0.8	2.58±0.5	516.0±30

It occurs that PU-NiTi800 is identified to reveal the highest tensile strength (19.7±0.8 MPa) and Young's modulus (2.58±0.8 MPa) as compared to the other two nanocomposite films. In Table 1, the percentage of elongation at break increases remarkably with PU-NiTi400 and PU-NiTi600 as given in entry 2 and 3, whereas the Young's modulus value drop for the same two samples. The stress-strain graphs (Fig. S15-S18) displayed almost identical curve profile in all four samples, elastic deformation of these films indicate only minimum elasticity behaviour. But the steady ramp in strain hardening region infers the modest plastic behaviour, particularly in PU-NiTi600 and PU-NiTi800 (Fig. S17 and S18).

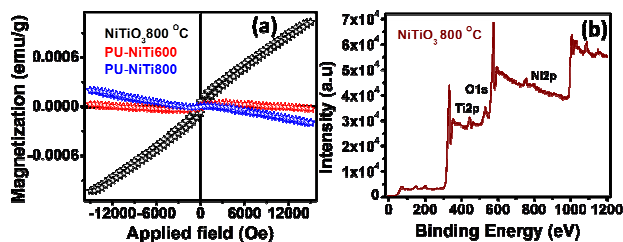


Fig. 5 a) *M-H* curves of NiTiO₃ NPs, PU-NiTi600 and PU-NiTi800 by VSM data and b) XPS data of NiTiO₃ after calcination at 800 °C.

Another representative study on NiTiO₃ NPs is the magnetic properties from VSM, depicted in Fig. 5a.⁸ NiTiO₃ NPs (calcinated at 800 °C) shows weak ferromagnetic properties. *M-H* profile of PU-NiTi600 revealed the suppressed magnetic behavior,⁶² presumably due to the lack of phase formation in NiTiO₃ at 600 °C. However, PU-NiTi800 is supposed to exhibit some evidence on reinforcement in magnetism, once if loading of NiTiO₃ exceeds its threshold limit.

In general, the monodispersity in size and shape of metal oxides essentially influences the magnetic properties. Nevertheless, the incorporation of NiTiO₃ NPs (0.5 wt. %) has not manifested any enhancement of magnetism in PU-NiTi600 and PU-NiTi800. The suppression in magnetism with PU-NiTi600 and PU-NiTi800 nanocomposite may have occurred due to the factors such as (i) the interaction between PU matrix with NiTiO₃ NPs may suppress the magnetic properties of the resulting nanocomposite films and (ii) presumably, the trace amount of NiTiO₃ NPs added in these film samples remain as ineffective to reinforce its magnetic properties. However, these findings justify the prospective interaction between PU and small proportion of NiTiO₃. The above interface is inferred as the minor deviation of magnetic curve towards diamagnetism.

To justify the stoichiometric formation of NiTiO₃, sample treated at 800 °C has been characterized by XPS spectrum to deduce the chemical state of the elements and its existence as shown in Fig. 5b. Binding energy of Ti2p with respect to Ti⁴⁺ ion was identified at 458 eV. This authenticates the absolute formation of Ti⁴⁺ ion free from any Ti³⁺ ion, which was corroborated by the absence of peak at 457 eV. Likewise, the existence of Ni²⁺ ion is represented by Ni2p signal at 802 eV.⁶³ Although the interpretation of O1s region is complicated due to the peak broadening and overlapping tendency with water and organic components, O1s peak of the above sample is manifested at 530 eV with respect to metal oxides, which always fit into 529-530 eV.^{37,63}

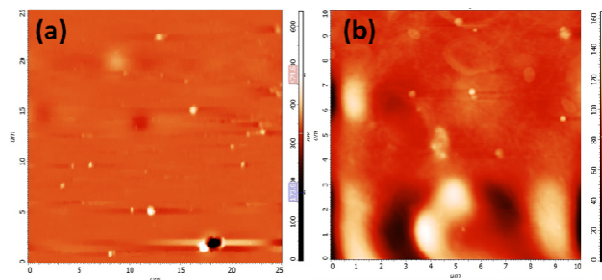


Fig. 6 AFM images a) NiTiO₃ NPs after calcination at 800 °C and b) PU-NiTi800 nanocomposite film.

The morphological feature of PU nanocomposite and NiTiO₃ was analyzed in images collected from SEM and AFM. SEM images are displayed in Fig. S4 (ESI), exhibit the topographic view of PU as well as the distribution of NiTiO₃ NPs on the surface of film. 2D image of NiTiO₃ NPs has been collected from AFM and displayed in Fig. 6a, which exhibits the wide variation in dimension of NPs, maximum height of 300 nm and width up to 1 μm. Fig. 6b depicts the AFM image of PU-NiTi800 film, supports the dispersion of NiTiO₃ NPs on PU with height profile of 100 nm on the basis of 2D image. The conclusion from 2D images were corroborated upon comparison with 3D images from AFM is shown in ESI. These images reveal the smooth surface without grains of nanoparticles and specify the height profile and roughness in terms of root mean square average (R_q). Fig. S5-S7 show the images of nanoparticles, whereas Fig. S8 and S11 show the roughness value of NiTiO₃ NPs

ARTICLE

RSC Advances

($R_q=8$ nm) and nanocomposite ($R_q=14$ nm). Fig. S9 and S10 magnify the region where NiTiO₃ NPs is incorporated with PU and Fig. S12-S14 exhibit the topographic view of these nanocomposite films. Altogether the images from both 2D and 3D images recorded from AFM are in good agreement with SEM images collected for the NiTiO₃ NPs and nanocomposite films.

The mechanism for the formation of PU-NiTiO₃ nanocomposite can be illustrated by the non-covalent interaction of NiTiO₃ *via* electronegative oxygen centres (O²⁻) and electropositive metal centres (Ni²⁺ and Ti⁴⁺). These charged species bind throughout the PU structural network, which could lead to the improvement in specific conductivity, thermal stability and mechanical properties.

In summary, slight shift in vibrational frequencies (Table S1, ESI) of functional groups in ATR-IR spectra of films suggests the facile interaction of NiTiO₃ with PU. In Raman spectra, among the amide I, amide II and amide III bands of urethane, amide I band shows fair shift in nanocomposite relative to PU. Amide II band does not shift, while the amide III and C=O band are disrupted due to the existence of NiTiO₃ in nanocomposite. In case of UV-*vis* DRS, no absorption is noticed in the visible region for the PU control film, whereas the nanocomposite films show absorption (549 and 551 nm) in the visible region infers the homogeneous distribution of NiTiO₃ on PU.

The improvement of specific conductivity ($8.72 \times 10^{-5} \text{ S cm}^{-1}$) of the PU-NiTiO₃ is about two order higher than the conductivity ($9.38 \times 10^{-7} \text{ S cm}^{-1}$) of PU. Thermal characterization of PU-NiTiO₃ by TGA shows elevation (>10 °C) of onset degradation temperature due to the incorporation of its intrinsic properties of NiTiO₃ on PU. DSC profile determines the thermal stability of nanocomposite films up to 300 °C, while the PU undergoes decomposition beyond 290 °C. PU-NiTiO₃ film exhibits plastic behaviour with enhanced tensile strength (19.7 ± 0.8 MPa), Young's modulus (2.58 ± 0.5 MPa) and elongation at break (516 ± 30 %), as compared to PU and other two PU-NiTiO₃ films. Since the trace amount of NiTiO₃ is loaded in PU-NiTiO₃ with effective interface, *M-H* profile depicts the suppression of magnetism towards diamagnetic, even if NiTiO₃ NPs exist as weak ferromagnetic. Morphological studies by AFM and SEM images were found to show good agreement with each other.

NiTiO₃ has been characterized by XRD, FT-IR, TGA, SEM, AFM, optical microscopic data and XPS spectrum, where binding energy of Ni2p (802 eV), Ti2p (458 eV) and O1s (530 eV) was noted to support the stoichiometric formation of NiTiO₃ at 800 °C. During calcination at 400, 600 and 800 °C, the pertinent rhombohedral phase formation of NiTiO₃ was attained at 800 °C, verified from JCPDS file number 33-690. Moreover, both Ti-O stretching mode and O-Ti-O bending mode of NiTiO₃ was noticed in FT-IR data.

4. Conclusions

In conclusion, rhombohedral phase NiTiO₃ NPs has been synthesized by sol-gel/co-precipitation method at 800 °C and loaded in trace amount (0.5 %) into PU matrix by *in situ* addition to cast as PU-NiTiO₃ nanocomposite films. Although these films are influenced by the least amount of NiTiO₃, film exhibits two order of increase in specific conductivity (10^{-5} S

cm^{-1}) relative to PU film ($10^{-7} \text{ S cm}^{-1}$), whereas TGA profile shows the enhancement in thermal stability in terms of shift in onset degradation temperature (>10 °C). In DSC data, the incorporation of NiTiO₃ has excluded the possibility of decomposition behaviour in nanocomposite films, which suggests the enhancement of thermal stability. The mechanical properties of these film samples are found to exhibit plastic behaviour. The anomalous magnetic feature was noticed from VSM, reveal the retardation in magnetism due to the existence of less amount of weak ferromagnetic NiTiO₃ NPs. The phase compatibility between inorganic metal oxide-polyurethane leads to the formation of potential nanocomposite films. Apart from the morphological characterization by optical, SEM and AFM images, ATR-IR, Raman, UV-*vis* DRS, XPS and XRD data support the unambiguous synthesis of the above samples, which could be appropriate to use as friction free coatings.

Acknowledgements

The first author (AM) thank Council of Scientific and Industrial Research, India Grant No: 31/6(389)/2013-EMR-I. The authors acknowledge the partial funding from Cross cluster project-ZERIS-WP21.

References

- 1 J. F. Scott, *Science*, 2007, **315**, 954-959.
- 2 F. Sánchez, C. Ocal and J. Fontcuberta, *Chem. Soc. Rev.*, 2014, **43**, 2272-2285.
- 3 C. Sanchez, B. Philippe, P. Michael and N. Lionel, *Chem. Soc. Rev.*, 2011, **40**, 696-753.
- 4 E. N. Armstrong, K. L. Duncan and E. D. Wachsman, *PCCP*, 2013, **15**, 2298-2308.
- 5 K. G. Reddy, T. G. Deepak, G. S. Anjusree, S. Thomas, S. Vadukumpully, K. R. V. Subramanian, S. V. Nair and A. S. Nair, *PCCP*, 2014, **16**, 6838-6858.
- 6 A. M. Banerjee, M. R. Pai, A. Arya and S. R. Bharadwaj, *RSC Adv*, 2015, **5**, 61218-61229.
- 7 D. Xu, L. Wang, W. Li, W. Wang, Y. Hou, W. Cao, Y. Feng and W. Fei, *PCCP*, 2014, **16**, 13078-13085.
- 8 S. Yuvaraj, V. D. Nitya, K. S. Fathima, C. Sanjeeviraja, G. K. Selvan, S. Arumugam and R. K. Selvan, *Mater. Res. Bull.*, 2013, **48**, 1110-1116.
- 9 T. Kirchartz, J. Bisquert, I. Mora-Sero and G. Garcia-Belmonte, *PCCP*, 2015, **17**, 4007-4014.
- 10 S. Protti, A. Albin, N. Serpone, *PCCP*, 2014, **16**, 19790-19827.
- 11 S. Royer, D. Duprez, F. Can, X. Courtois, C. Batiot-Dupeyrat, S. Laassiri and H. Alamdari, *Chem. Rev.*, 2014, **114**, 10292-10368.
- 12 W. Wang, M. O. Tadé and Z. Shao, *Chem. Soc. Rev.*, 2015, **44**, 5321-5408.
- 13 T. Kirchartz, J. Bisquert, I. Mora-Sero and G. Garcia-Belmonte, *PCCP*, 2015, **17**, 4007-4014.
- 14 H. Sun, Y. Jiang, L. Qiu, X. You, J. Yang, X. Fu and H. Peng, *J. Mater. Chem. A*, 2015, **3**, 14977-14984.

- 15 J. C. Ruiz-Morales, J. Canales-Vázquez, C. Savaniu, D. Marrero-López, P. Núñez, W. Zhou and J. T. Irvine, *PCCP*, 2007, **9**, 1821-1830.
- 16 X. Z. Li, H. Liu, L. F. Cheng and H. J. Tong, *Environ. Sci. Technol.*, 2003, **37**, 3989-3994.
- 17 G. Dong, H. Fan, H. Tian, J. Fang and Q. Li, *RSC Adv.*, 2015, **5**, 29618-29623.
- 18 K. Friedrich and A. K. Schlarb, Tribology of polymeric nanocomposites: friction and wear of bulk materials and coatings. *Elsevier*, 2011, **55**, 1-543.
- 19 Y. Ni, X. Wang, J. Hong, *Mater. Res. Bull.* 2009, **44**, 1797-1801.
- 20 W. Li, H. Dong, L. Wang, N. Li, X. Guo, J. Li and Y. Qiu, *J. Mater. Chem. A*, 2014, **2**, 13587-13592.
- 21 A. Fuertes, *J. Mater. Chem.*, 2012, **22**, 3293-3299.
- 22 H. Althues, J. Henle and S. Kaskel, *Chem. Soc. Rev.*, 2007, **36**, 1454-1465.
- 23 E. Badamshina, Y. Estrin and M. Gafurova, *J. Mater. Chem. A*, 2013, **1**, 6509-6529.
- 24 R. Ciriminna, A. Fidalgo, V. Pandarus, F. Béland, L. M. Ilharco and M. Pagliaro, *Chem. Rev.*, **113**, 6592-6620.
- 25 Y. Xia and R. C. Larock, *Macromol. Rapid Commun.*, 2011, **32**, 1331-1337.
- 26 T. Gurunathan, S. Mohanty and S. K. Nayak, *RSC Adv.*, 2015, **5**, 11524-11533.
- 27 W. K. Chee, H. N. Lim, N. M. Huang and I. Harrison, *RSC Adv.*, 2015, **5**, 68014-68051.
- 28 Z. Guo, C. Yang, H. Wei, Y. Wang, J. Guo, Y. Xingru and Z. Xi, *J. Mater. Chem. A*, 2015, **3**, 14929-14941.
- 29 K. M. Seenii Meera, R. Murali Sankar, S. N. Jaisankar and A. B. Mandal, *J. Phys. Chem. B*, 2013, **117**, 2682-2694.
- 30 M. Sagar, S. Balakumar, I. Bhaumik, P. K. Gupta and S. N. Jaisankar, *RSC Adv.*, 2014, **4**, 16871-16878.
- 31 P. Murugan, M. Krishnamurthy, S. N. Jaisankar, D. Samanta and A. B. Mandal, *Chem. Soc. Rev.*, 2015, **44**, 3212-3243.
- 32 K. M. S. Meera, R. M. Sankar, J. Paul, S. N. Jaisankar and A. B. Mandal, *PCCP*, 2014, **16**, 9276-9288.
- 33 R. M. Sankar, K. M. S. Meera, A. B. Mandal and S. N. Jaisankar, *High Perform. Polym.*, 2013, **25**, 135-146.
- 34 D. Samanta, R. M. Sankar, S. N. Jaisankar, M. S. Alam and A. B. Mandal, *Chem. Commun.*, 2011, **47**, 11975-11977.
- 35 A. Murali, S. A. Gurusamy-Thangavelu, S. N. Jaisankar and A. B. Mandal, *RSC Adv.*, 2014, **4**, 62947-62950.
- 36 A. V. Murugan, V. Samuel, S. C. Navale and V. Ravi, *Mater. Lett.*, 2006, **60**, 1791-1792.
- 37 A. B. Gambhire, M. K. Lande, S. B. Kalokhe, A. B. Mandale, K. R. Patil, R. S. Gholap and B. R. Arbad, *Phil. Mag. Lett.*, 2008, **88**, 467-472.
- 38 R. S. Singh, T. H. Ansari, R. A. Singh and B. M. Wanklyn, *Mater. Chem. Phys.*, 1995, **40**, 173-177.
- 39 D. L. Reid, R. Draper, D. Richardson, A. Demko, T. Allen, E. L. Petersen and S. Seal, *J. Mater. Chem. A*, 2014, **2**, 2313-2322.
- 40 N. Dharmaraj, H. C. Park, C. K. Kim, H. Y. Kim and D. R. Lee, *Mater. Chem. Phys.*, 2004, **87**, 5-9.
- 41 S. Khanahmadzadeh, S. Simani, M. Enhessari and B. Khezri, *IPCBE*, 2012, **43**, 31.
- 42 I. S. Chronakis, *J. Mater. Process Tech.*, 2005, **167**, 283-293.
- 43 M. Lakshmi, R. S. Aashish, K. Syed, F. Muhammad, K. C. Sajjan and M. Revanasiddappa, *AIP Adv.*, 2013, **3**, 112-113.
- 44 G. Zhao, W. Tingmei and W. Qihua, *J. Mater. Sci.*, 2011, **46**, 6673-6681.
- 45 Y. I. Estrin, E. R. Badamshina, A. A. Grishchuk, G. S. Kulagina, V. A. Lesnichaya, Y. A. Ol'khov, A. G. Ryabenko and S. N. Sul'yanov, *Polym. Sci. Ser. A*, 2012, **54**, 290-298.
- 46 L. Zhu and Q. Wang, *Macromolecules*, 2012, **45**, 2937-2954.
- 47 G. Trovati, E. A. Sanches, S. C. Neto, Y. P. Mascarenhas and G. O. Chierice, *J. Appl. Polym. Sci.*, 2010, **115**, 263-268.
- 48 S. N. Jaisankar, D. J. Nelson and C. N. Brammer, *Polymer*, 2009, **50**, 4775-4780.
- 49 M. Mirzaee, and M. M. Amini, *Appl. Organomet. Chem.*, 2005, **19**, 339-342.
- 50 Y. Deng, Q. Lv, S. Wu and S. Zhan, *Dalton Trans.*, 2010, **39**, 2497-2503.
- 51 Y. Ni, X. Wang and J. Hong, *Mater. Res. Bull.*, 2009, **44**, 1797-1801.
- 52 H. J. Kitchen, S. R. Vallance, J. L. Kennedy, N. Tapia-Ruiz, L. Carassiti, A. Harrison and D. H. Gregory, *Chem. Rev.*, 2013, **114**, 1170-1206.
- 53 K. Huang, M. Feng and J. B. Goodenough, *J. Am. Ceram. Soc.*, 1996, **9**, 1100-1104.
- 54 A. E. Henkes, J. C. Bauer, A. K. Sra, R. D. Johnson, R. E. Cable and R. E. Schaak, *Chem. Mater.*, 2006, **18**, 567-571.
- 55 S. Anandan, T. Lana-Villarreal and J. J. Wu, *Ind. Eng. Chem. Res.*, 2015, **54**, 2983-2990.
- 56 D. R. Modeshia and R. I. Walton, *Chem. Soc. Rev.*, 2011, **39**, 4303-4325.
- 57 J. H. Kim, K. Zhu, Y. Yan, C. L. Perkins and A. J. Frank, *Nano Lett.*, 2010, **10**, 4099-4104.
- 58 K. P. Lopes, L. S. Cavalcante, A. Z. Simões, J. A. Varela, E. Longo and E. R. Leite, *J. Alloy Comp.*, 2009, **468**, 327-332.
- 59 Y. J. Lin, Y. H. Chang, W. D. Yang and B. S. Tsai, *J. Non-Cryst. Solids*, 2006, **352**, 789-794.
- 60 Y. Lu and R. C. Larock, *Biomacromolecules*, 2008, **9**, 3332-3340.
- 61 S. A. Gurusamy-Thangavelu, S. J. Emond, A. Kulshrestha, M. A. Hillmyer, C. W. Macosko, W. B. Tolman and T. R. Hoye, *Polym. Chem.*, 2012, **3**, 2941-2948.
- 62 C. J. Fennie, *Phys. Rev. Lett.*, 2008, **100**, 167203.
- 63 V. V. Atuchin, G. K. Valery, V. P. Natalia and Z. Zhaoming, *J. Electron Spectrosc. Relat. Phenom.*, 2006, **152**, 18-24.

Enhancement of physicochemical properties of polyurethane-perovskite nanocomposite *via* addition of nickel titanate nanoparticles

Adhigan Murali,^a Senthil A. Gurusamy-Thangavelu,^{a,*} Sellamuthu N. Jaisankar^{a,*} and Asit Baran Mandal^{a,b*}

^aPolymer Division, ^bChemical laboratory, Council of Scientific and Industrial Research (CSIR)-CLRI, Adyar, Chennai-600 020, India. *E-mail: senthil@clri.res.in; snjsankar@clri.res.in; abmandal@clri.res.in; Tel: 91-44-24422059; Fax: 91-44-24911589.

Perovskite (NiTiO₃ NPs) is integrated with polyurethane (PU) by *in situ* addition to form unprecedented nanocomposite films (~1.5 mm). The pertinent rhombohedral phase of NiTiO₃ has been achieved at 800 °C, loaded in trace amount (0.5 wt. %) to explore its influence on PU matrix, which enhances their thermal stability, electrical conductivity and mechanical strength as well as the effect in magnetic and optical properties.

